Supplementary Information (SI) for Journal of Materials Chemistry C.
This journal is © The Royal Society of Chemistry 2025

Supporting Information on

Density functional theory and EXAFS spectroscopy studies of formamidoxime intercalated molybdenum disulfide for the removal of Eu(III) and U(VI)

Jian Wang*, Wangyang Liu, Yan Li

MOE Key Laboratory of Resources and Environmental System Optimization, College of Environmental Science and Engineering, North China Electric Power University, Beijing, 102206, P.R. China

*: Corresponding author. Email: wangjian@ncepu.edu.cn (J. Wang).

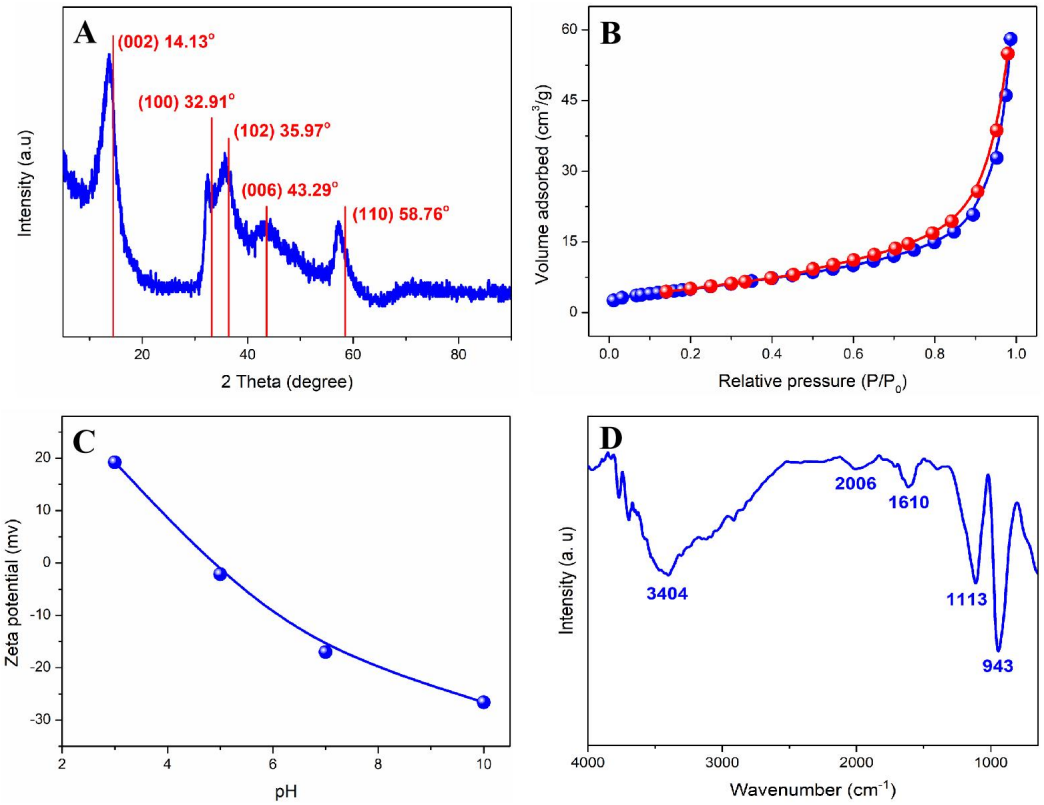

Figure S1. The XRD pattern (A), N_2 sorption-desorption isotherms (B), zeta potential (C), and FTIR spectrum (D) of CH_4N_2O-MoS_2.

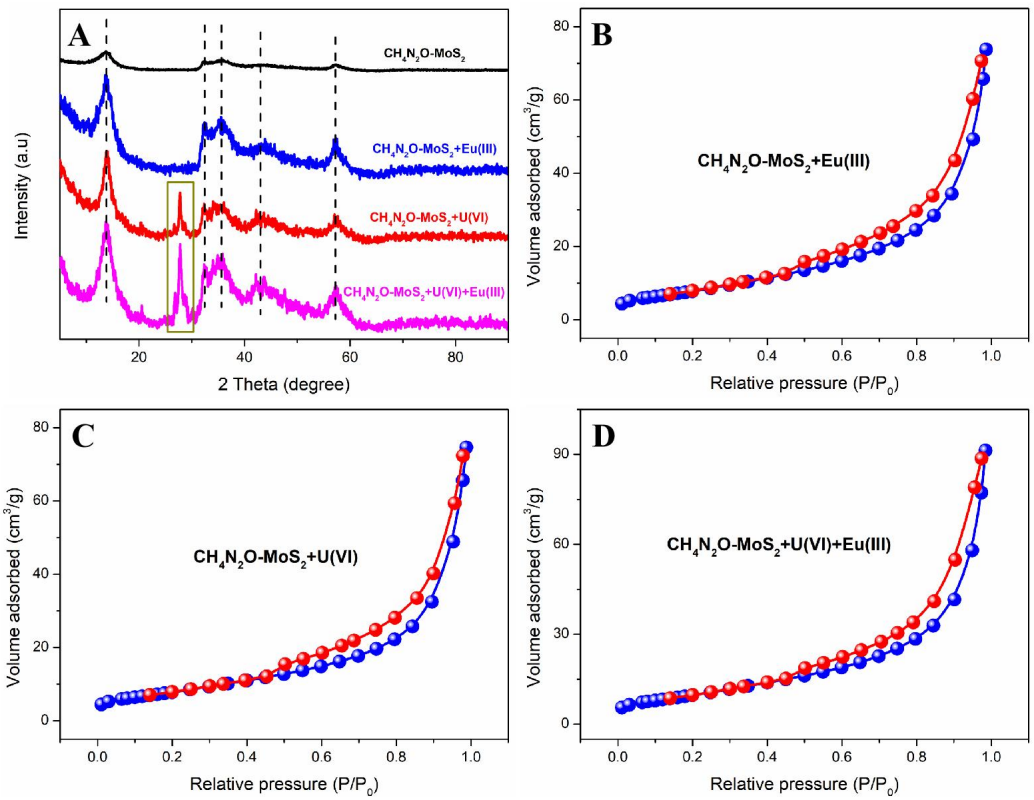

Figure S2. The XRD patterns of CH_4N_2O-MoS_2 before and after adsorption (A); N_2 sorption-desorption isotherms of CH_4N_2O-MoS_2 after Eu(III) (B), U(VI) (C), and Eu(III)+U(VI) (D) removal.

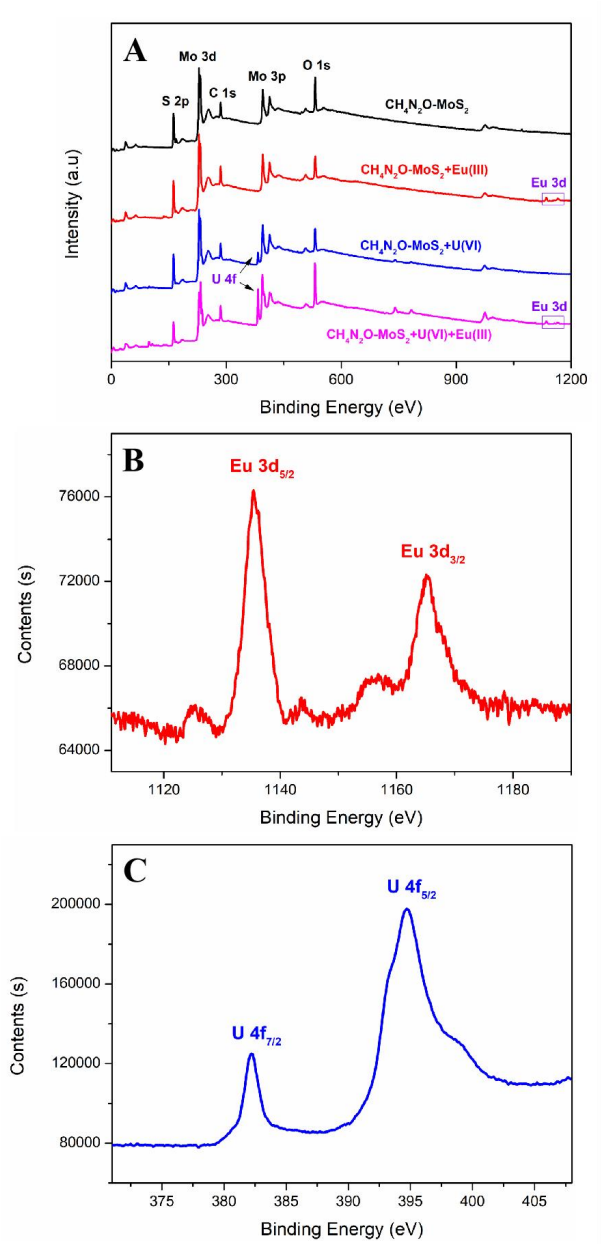

Figure S3. XPS spectra: the wide scan of CH_4N_2O-MoS_2 before and after adsorption (A); the peaks for Eu 3d (B) and U 4f (C).

Batch Adsorption Experiments

In the adsorption experiment, the Eu(III) stock solution was derived from europium nitrate hexahydrate. A certain amount of H_4N_2O-MoS_2 (60 mg), Eu(III) stock solution, and NaCl solution were added to the Erlenmeyer flask (250 mL). The concentrations of Eu(III) and NaCl were kept at 100 mg/L and 0.01 M, respectively. The solid-to-liquid ratio was kept at 1.0 g/L, and the pH was maintained at 5.0±0.2 by using 0.1-0.01 M HCl or NaOH. The Erlenmeyer flask was shocked at 100 rpm for 12 hours. After separation, the concentration of Eu(III) was detected by an inductively coupled plasma spectrometer (Agilent 5110, ICP-OES). The adsorption of U(VI) on H_4N_2O-MoS_2 also followed the above steps. The removal capacity of CH_4N_2O-MoS_2 for Eu(III) or U(VI) can be expressed as:

$$q_e = \frac{(C_0 - C_e)V}{m} \tag{1}$$

where q_e (mg/g) is the adsorption capacity, m (g) is the material mass, V (L) is the solution volume, C_0 and C_e (mg/L) are the original and equilibrium concentrations of Eu(III) or U(VI).

The pseudo-first-order kinetic can be expressed as:

$$ln(q_e - q_t) = ln\, q_e - k_1 t \tag{2}$$

The pseudo-second-order kinetic is expressed as:

$$q_t = \frac{k_2 q_e^2 t}{1 + k_2 q_e t} \tag{3}$$

where q_t and q_e (mg/g) represent the quantities of contaminant adsorbed on CH_4N_2O-MoS_2 at time t (min) and equilibrium; k_1 and k_2 represent the corresponding

adsorption rate constants.

The *Langmuir* model is described as:

$$q_e = \frac{Q_0 C_e b}{1 + C_e b} \tag{4}$$

The *Freundlich* model is expressed as:

$$q_e = K_f C_e^{1/n} \tag{5}$$

where Q_0 (mg/g) denotes the theoretical saturated adsorption capacity; q_e (mg/g) is the adsorption capacity; b (L/mg) represents the *Langmuir* constant; K_f (mg/g) and n are *Freundlich* coefficients; C_e (mg/L) represents the equilibrium concentration of the contaminant.

Table S1. The pseudo-first-order kinetic model and pseudo-second-order kinetic model for Eu(III) and U(VI) adsorption.

	Pseudo-first-order kinetic model		Pseudo-second-order kinetic model	
Contaminant	R^2	k_1	R^2	k_2
Eu(III)	0.975	0.074	0.973	0.053
U(VI)	0.982	0.035	0.959	0.027

Table S2. The adsorption capacity of CH_4N_2O-MoS_2 compared with other materials.

Pollutant	Adsorbent	q_e (mg/g)	Reference
Eu(III)	MoS_2	48.6	[1]
Eu(III)	biopolymer chitosan-yeast combination	19.41	[2]
Eu(III)	Al-substituted goethite	6.75	[3]
Eu(III)	CMPEI/MCM-48	64.9	[4]
Eu(III)	CMC/MMWCNTs	51.1	[5]
Eu(III)	CH_4N_2O-MoS_2	69.8	This study
U(VI)	MoS_2	66.5	[1]
U(VI)	Chitosan	22.3	[6]
U(VI)	Graphene Oxide	75.71	[7]
U(VI)	SDS/MoS_2	98.4	[1]
U(VI)	CH_4N_2O-MoS_2	137.1	This study

Table S3. Comparison of BET surface areas and pore diameters of CH_4N_2O-MoS_2 before and after adsorption.

System	BET surface area (m^2/g)	Pore volume (cm^3/g)	Average pore diameter (nm)
CH_4N_2O-MoS_2	19.1	0.090	18.89
CH_4N_2O-MoS_2+Eu(III)	30.1	0.114	15.21
CH_4N_2O-MoS_2+U(VI)	29.4	0.116	15.74
CH_4N_2O-MoS_2+Eu(III)+U(VI)	36.9	0.141	15.35

Theoretical calculations

All calculations in this study were performed with the Vienna ab initio Simulation Package (VASP) [8] within the frame of density functional theory (DFT). The exchange-correlation interactions of electrons were described via the generalized gradient approximation (GGA) with PBE functional [9], and the projector augmented wave (PAW) method [10] was used to describe the interactions of electrons and ions. Additionally, the DFT-D3 method [11, 12] was used to account for the long-range van der Waals forces present within the system. The Monkhorst-Pack scheme [13] was used for the integration in the irreducible Brillouin zone. The kinetic energy cut-off of 450 eV was chosen for the plane wave expansion. The lattice parameters and ionic position were fully relaxed, and the total energy was converged within 10^{-5} eV per formula unit. The final forces on all ions are less than 0.02/Å. The adsorption energy (E_{ad}) can be calculated as:

$$E_{ad} = E_{CH4N2O\text{-}MoS2} + E_{U(VI)} - E_{CH4N2O\text{-}MoS2\text{-}U(VI)} \quad (6)$$

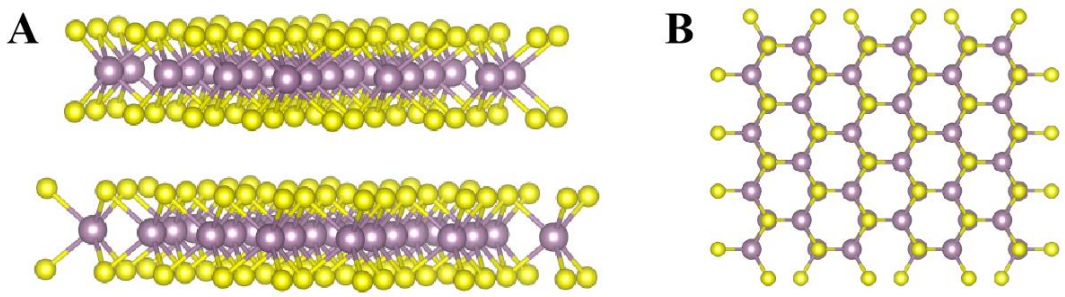

Figure S4. Front view (A) and top view (B) of optimized molecular structures for MoS_2.

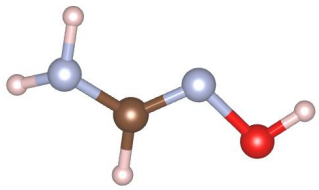

Figure S5. Optimized molecular structure of CH_4N_2O.

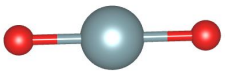

Figure S6. Optimized molecular structure of U(VI) (UO_2^{2+}).

EXAFS analysis background

The obtained XAFS data was processed in Athena (version 0.9.26) [14] for background, pre-edge line, and post-edge line calibrations. Then Fourier transformed fitting was carried out in Artemis (version 0.9.26) [14]. The k^3 weighting, k-range of 3- ~11.5 $Å^{-1}$, and R range of 1-3 Å were used for the fitting of $EuCl_3$. The k^3 weighting, k-range of 3-~10.5 $Å^{-1}$, and R range of 1-3 Å were used for the fitting of the sample. The k^3 weighting, k-range of 3-12 $Å^{-1}$, and R range of 1-3 Å were used for the fitting of $UO_2(NO_3)_2$. The k^3 weighting, k-range of 3-~11.5 $Å^{-1}$, and R range of 1-3 Å were used for the fitting of the sample. For wavelet transform analysis, the $\chi(k)$ exported from Athena was imported into the Hama Fortran code [15]. The parameters were listed as follows: R range, 0-4 Å; k range, 0-16 $Å^{-1}$. Morlet function with κ=10, σ=1 was used as the mother wavelet to provide the overall distribution [16].

References

[1] Wang, J., Yang, S., Cheng, G., Gu, P., 2020. The Adsorption of Europium and Uranium on the Sodium Dodecyl Sulfate Modified Molybdenum Disulfide Composites. J. Chem. Eng. Data 65, 2178-2185.

[2] Arunraj, B., Talasila, S., Rajesh, V., Rajesh, N., 2019. Removal of Europium from aqueous solution using Saccharomyces cerevisiae immobilized in glutaraldehyde cross-linked chitosan. Separ. Sci. Technol. 54, 1620-1631.

[3] Li, M., Liu, H., Chen, T., Hayat, T., Alharbi, N.S., Chen, C., 2017. Adsorption of

Europium on Al-substituted goethite. J. Mol. Liq. 236, 445-451.

[4] Yun, M.H., Yeon, J.W., Kim, J.H., Lee, H.I., Kim, J.M., Kim, S., Jung, Y., 2011. Preparation and application of chelating polymer-mesoporous silica composite for Europium-ion adsorption. Macromol. Res. 19, 421-426.

[5] Zong, P., Cao, D., Cheng, Y., Wang, S., Hayat, T., Alharbi, N.S., Guo, Z., Zhao, Y., He, C., 2018. Enhanced performance for Eu(iii) ion remediation using magnetic multiwalled carbon nanotubes functionalized with carboxymethyl cellulose nanoparticles synthesized by plasma technology. Inorg. Chem. Front. 5, 3184-3196.

[6] Xu, J., Chen, M., Zhang, C., Yi, Z., 2013. Adsorption of uranium(VI) from aqueous solution by diethylenetriamine-functionalized magnetic chitosan. J. Radioanal. Nucl. Ch. 298, 1375-1383.

[7] Zhao, Z.W., Li, J.X., Wen, T., Shen, C.C., Wang, X.K., Xu, A.W., 2015. Surface functionalization graphene oxide by polydopamine for high affinity of radionuclides. Colloid. Surface. A 482, 258-266.

[8] Kresse, G., Furthmuller, J. Efficient Iterative Schemes for Ab Initio Total-Energy calculations Using a Plane-Wave Basis Set. Phys. Rev. B. 1996, 54, 11169-11186.

[9] Perdew, J. P., Burke, K. & Ernzerhof, M. Generalized gradient approximation made simple. Phys. Rev. Lett. 1996, 77, 3865-3868.

[10] Kresse, G., Joubert, J. From Ultrasoft Pseudopotentials to the Projector Augmented-Wave Method. Phys. Rev. B. 1999, 59, 1758-1775.

[11] Grimme, S., Antony, J., Ehrlich, S., Krieg, H. A consistent and accurate ab initio parametrization of density functional dispersion correction (DFT-D) for the 94

elements H-Pu. J. Chem. Phys. 2010, 132.

[12] Grimme, S., Ehrlich, S., Goerigk, L. Effect of the damping function in dispersion corrected density functional theory. J Comput Chem 2011, 32, 1456-1465.

[13] Monkhorst, H. J., Pack, J. D. Special points for Brillouin-zone integrations. Phys. Rev. B. 1976, 13, 5188-5192.

[14] Ravel, B., Newville, M. ATHENA, ARTEMIS, HEPHAESTUS: data analysis for X-ray absorption spectroscopy using IFEFFIT. J. Synchrotron Rad. 2005, 12, 537-541.

[15] Funke, H.; Scheinost, A. C.; Chukalina, M. Wavelet analysis of extended X-ray absorption fine structure data. Physical Review 2005, B 71, 094110.

[16] Funke, H.; Chukalina, M.; Scheinost, A. C. A new FEFF-based wavelet for EXAFS data analysis. Journal of Synchrotron Radiation 2007, 14, 426-432.